PALEOCEANOGRAPHY, VOL. 9, NO. 6, PAGES 897-916, DECEMBER 1994

Modeling sediment drifts: A coupled oceanic circulation–sedimentation model of the northern North Atlantic

Bernd J. Haupt, Christian Schäfer-Neth, and Karl Stattegger

Geological-Paleontological Institute and Special Research Project 313, University of Kiel, Kiel Germany

Abstract. Modeling of sediment drifts in the northern North Atlantic is achieved by coupling the ocean general circulation model sensitivity and circulation in the northern North Atlantic (SCINNA) to the sedimentation models sedimentation in the northern North Atlantic (SENNA) and particle tracing in the northern North Atlantic (PATRINNA). SCINNA is based on the primitive equations with conservation of mass, momentum, heat, and salt. SENNA and PATRINNA are driven by temperature, salinity, and velocity fields derived from SCINNA. Sediments are supplied from the surface and from the continental margins. The modeling includes three–dimensional sediment transport in the water column and two–dimensional processes in a thin bottom layer. Sediments are allowed to resuspend repeatedly, thus offering the possibility of stepwise transport. SENNA calculates erosion, transport, and deposition of sediments, resulting in sedimentation patterns for specific time intervals. PATRINNA models the transport paths of single sediment grains corresponding to the ocean circulation. Sensitivity experiments for the modern state and for the last glacial maximum show differences in the large sediment drifts between the Charlie Gibbs Fracture Zone and the Greenland–Scotland Ridge for these two time slices. The sediment supply changes with the differing circulation modes and is strongly constrained by topography.

Introduction

Sediment waves and sediment drifts are prominent features used in recognizing deep water circulation from deep–sea sediments. Sedimentation rates and mass–age distributions of sediment drifts are also used to reconstruct paleocirculation patterns from the sedimentary record.

The thermohaline circulation system drives the sedimentary system of erosion transport deposition in oceanic basins. Therefore numerical modeling of the oceanic circulation coupled with a sedimentary system model should prove useful in simulating basinwide sedimentation patterns, following the path of sediments from the input to the ocean (terrigenous) or production in the ocean (biogenic) to the place of final deposition. Medium–to–large–scale sediment drifts are particularly likely to be realistically simulated from three–dimensional velocity–temperature–salinity fields of a suitable oceanic general circulation model (OGCM), considering preexisting topography, sediment supply, grain size, and bottom friction in the sedimentation model. Such models must be able to operate (1) in a basinwide range of several thousands of kilometers; (2) with high–resolution topography; and (3) for long time intervals covering several thousands to millions of years of the sedimentary system after reaching a quasi–equilibrium state in the oceanic circulation.

In the northern North Atlantic (NNA), large–scale sediment drifts include the Feni Drift, Hattar Drift, Bjorn Drift, Gadar Drift, Snorri Drift, Eirik Drift, and Gloria Drift [*McCave and Tucholke*, 1986; *Wold*, 1992; this issue] (Figure 1). These sediment drifts between the Charlie Gibbs Fracture Zone and the Greenland–Scotland Ridge result from the equatorially directed thermohaline deepwater circulation deflected to the west by the Coriolis force. The currents of this circulation system are intensified and further modified in their direction by topographic highs. Such contour currents erode and transport sediments at higher velocities depending on the grain size and deposit them as drifts where the velocity decreases.

During the Late Quaternary the circulation pattern in the NNA changed several times due to varying climatologic forcing, as reconstructions from proxy data [*Sarnthein et al.*, 1992] and from numerical modeling [*Keir et al.*, 1993] show. Different modes of the oceanic

Paper number 94PA01437.
0883-8305/94/94PA-01437$10.00

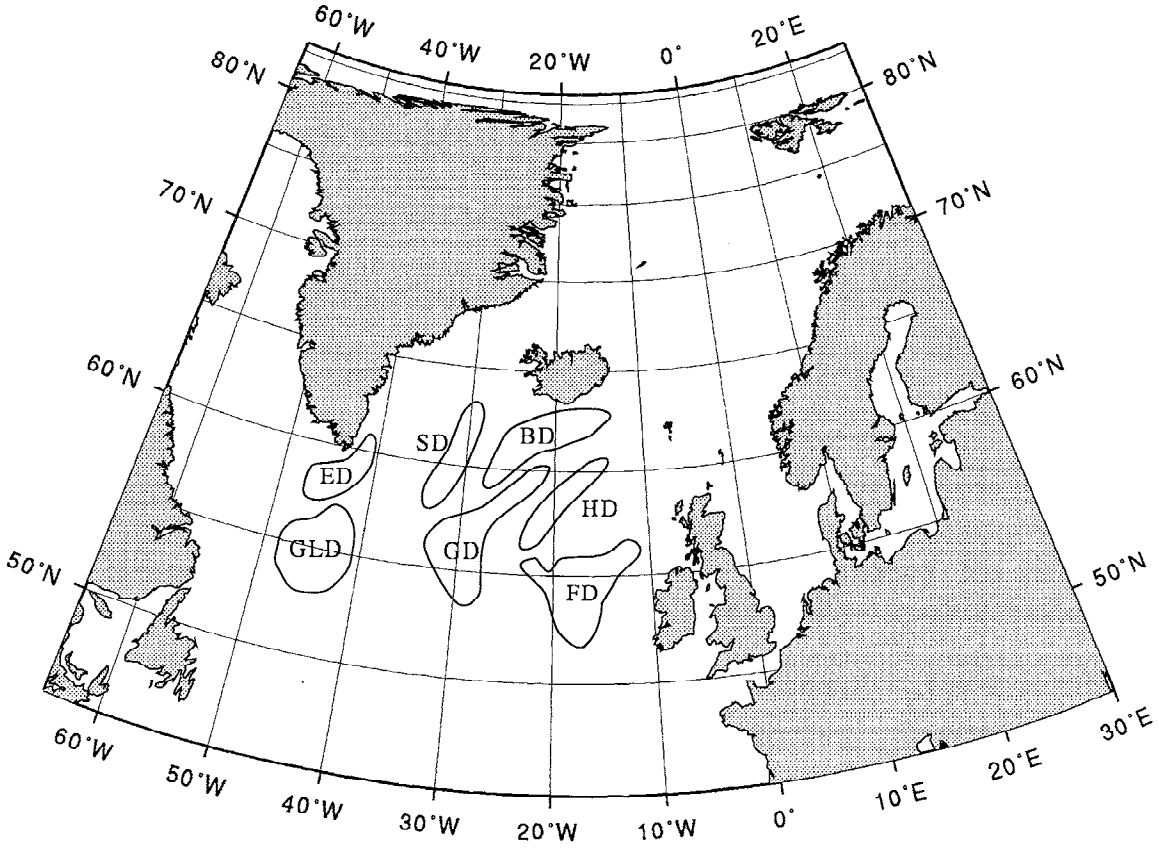

Figure 1. Sediment drifts in the northern North Atlantic. GLD, Gloria Drift; ED, Eirik Drift; SD, Snorri Drift; GD, Gadar Drift; BD, Bjorn Drift; HD, Hattar Drift; FD, Feni Drift.

circulation generate different modes of the sedimentary system with different patterns of sediment drifts. These features should show up in numerical models. This study concerning sediment drifts in the NNA aims to (1) realistically simulate the modern NNA circulation; (2) couple a suitable sedimentation model to the OGCM; (3) validate the simulated modern sedimentation patterns with the observed ones; (4) trace individual sediment particles through space and time; (5) conduct sensitivity tests for the development of high–accumulation areas (sediment drifts); and (6) simulate different ocean circulation modes and resulting sedimentation patterns corresponding to the paleoceanographic record.

Existing models do not fullfill these aims. In particular, the coupling of OGCMs and sedimentation models to simulate sedimentation processes in a large oceanic basin has not been attempted for a real ocean so far. The new approach presented here is thus chosen to give a better understanding as to the origin and evolution of large sediment bodies such sediment drifts.

Models and Model Area

Considering the modeling goals and the specific regional setting outlined above, three numerical models were developed: (1) SCINNA, sensitivity and circulation in the northern North Atlantic; (2) SENNA, sedimentation in the northern North Atlantic; and (3) PATRINNA, particle tracing in the northern North Atlantic.

These models are coupled in the following way: First, SCINNA calculates the oceanic circulation. The modeled circulation then initializes SENNA and PATRINNA: SENNA simulates the general sedimentation pattern governed by erosion, transport, and accumulation processes, whereas PATRINNA simulates the transport paths of single sediment grains.

In general, an inverse procedure is used. The solutions of the forward models optimize the matching of predictions and existing data. SCINNA uses data–based temperature, salinity, ice, and wind speed distributions to calculate the oceanic circulation. SENNA and PATRINNA use the model circulation with the resulting velocity fields to calculate erosion, transport, and deposition of sediments. The forward models run multiple times, each time comparing model predictions to the data and adjusting the temperature–salinity reconstructions progressively if the quality of the data is high compared to the sensitivity of the models (Figure 2). Measured data and proxy data constrain the models' solutions. However, the errors present in the data increase the confidence limits of the model results.

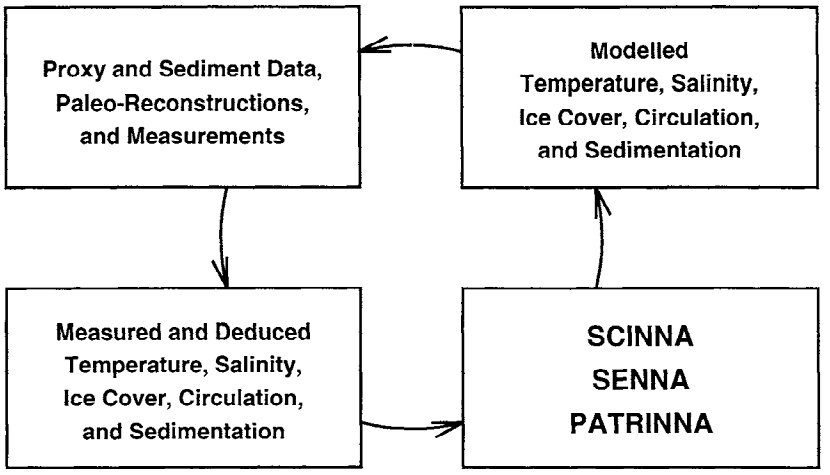

Figure 2. Inverse method for reconstructing the ocean's state.

Conversely, the physically consistent models point out possible inconsistencies in the data and their confidence limits. The influence and the validity of single parameters and variables on the modeled system can successfully be proved by sensitivity experiments.

Model Area

SCINNA, SENNA, and PATRINNA use the same grid and topography, covering the northern North Atlantic, the Norwegian–Greenland Seas, the Barents Sea, and parts of the Polar Basin. The coordiante system is a spherical one, similar to normal geographical coordinates, where the equator has been rotated northward by 60 deg along zero meridian. As a minor complication, the coriolis force depends on both latitude and longitude in this system. On the other hand, the convergence of meridians is minimized by the rotation. Conventional geographical coordinates would yield a very narrow grid

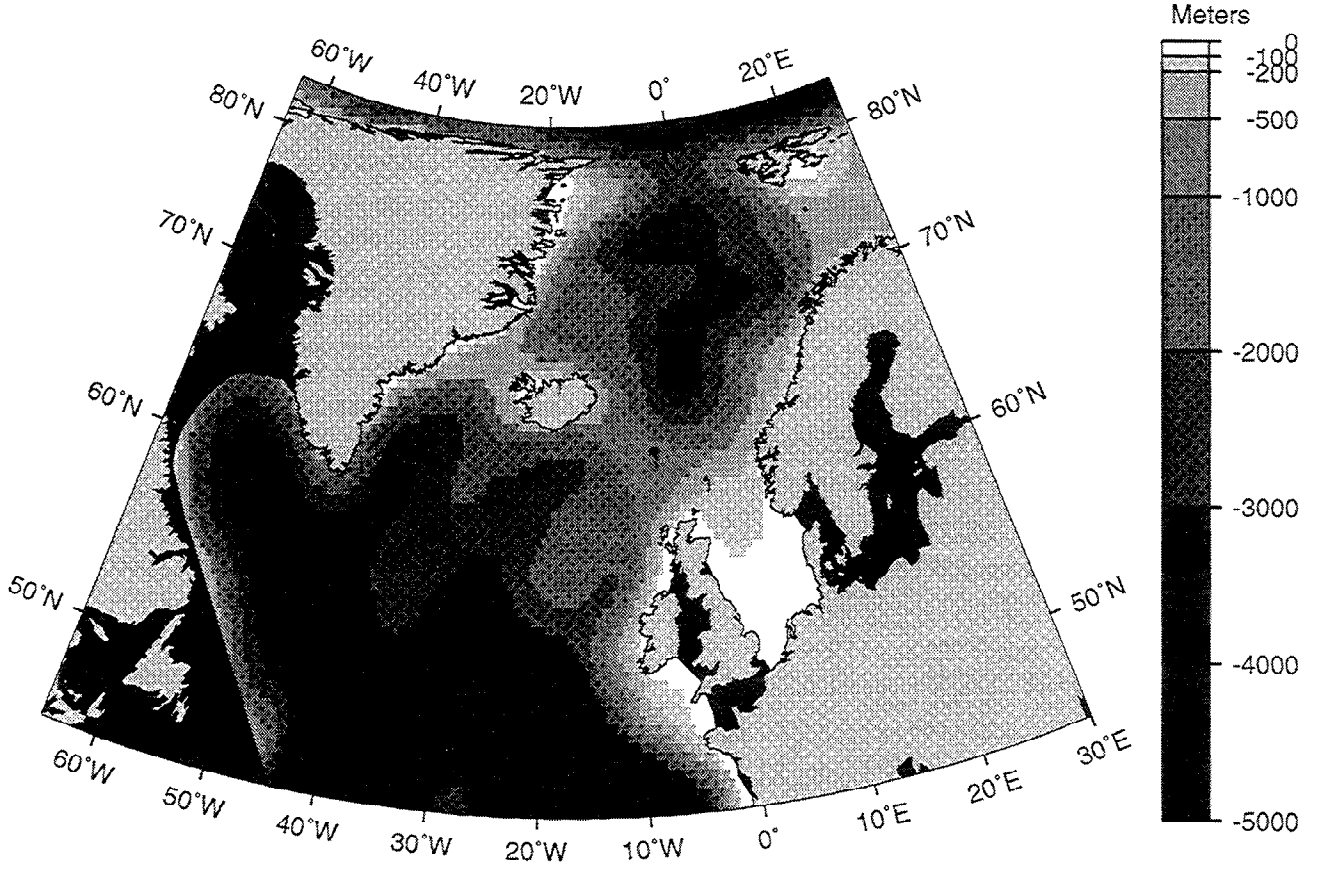

Figure 3. Modern model topography.

spacing in the model's northern regions and in turn require very short time steps. The rotated coordinates are quite inconvenient to recognize. Therefore we present our results in a more familiar equal area projection. With rotation, a horizontal resolution of 0.5 deg and 95 grid points in both directions, the spacing is about 50 kilometers everywhere, and time steps of 12 hours for tracers and 30 min for velocities can be used. The vertical is split into 17 levels, so that topography can be represented in a realistic manner (Figure 3):

Level	Depth, m
1	50
2	100
3	150
4	200
5	300
6	400
7	500
8	750
9	1000
10	1250
11	1500
12	2000
13	2500
14	3000
15	3500
16	4000
17	5000

SCINNA

In principle, the state of the Norwegian–Greenland Seas cannot successfully be modeled without taking into account the influence of the complete world ocean, especially it's transformation of water masses. However, limited computer resources restrict the resolution of global models. Consequently, SCINNA covers only a very small part of the world ocean, which necessitates the introduction of artificial boundaries where parts of the ocean have been clipped off.

There are essentially two ways to incorporate the effects of the discarded regions:

1. these boundaries can be modeled as open boundaries, allowing both inflow and outflow, which must be carefully specified. The model's state depends critically on the positions of the flows across the margins, as well as their mass, heat, and salt transports. This has been shown recently by the work of *Stevens* [1991] and *Legutke* [1989]. For past time slices, transport estimates from proxy data do not exist, and open boundaries cannot be employed in this manner.

2. the boundaries can be kept closed. Initially, this appears even more unrealistic, but placing the closed walls far away from the area of interest minimizes any unrealistic features. Furthermore, the use of restoring zones along the closed walls re–introduces the world ocean's water mass transformation. These zones comprise 300 km wide bands along the artificially closed boundaries, the North Sea, the Baffin Bay, and the coast of Novaya Zemlya, where the temperatures and salinities are forced to prescribed values with some given time constant. Thus, for example, cold deep water entering the restoring area at the southern closed margin will be upwelled and leave it as warm surface water going northwards. This technique is used in SCINNA and yields realistic results for the modern circulation and water mass distribution in the Norwegian–Greenland Seas. On the other hand, paleoreconstructions of temperatures and salinities are available and can be used for restoring purposes when modeling the paleocirculation [*Duplessy et al.*, 1991; *Sarnthein et al.*, 1992; *Pflaumann*, 1985; U. Pflaumann et al., SIMMAX, a transfer technique to deduce Atlantic sea surface temperatures from planctonic foraminifera — the "EPOCH" approach, submitted to *Paleoceanography*, 1994]. Therefore the closed boundary/restoring approach is well suitable for paleo–modeling. Such an approach is used as well by Aukrust and Oberhuber [Modeling of the Greenland, Iceland and Norwegian Seas with a coupled sea ice — mixed layer — isopycnal ocean model, submitted to *Journal of Geophysical Research*, 1994] in their model of the (modern) Atlantic, which is driven by heat and freshwater fluxes. However, flux data have not been reconstructed for past times, so SCINNA is forced by sea surface temperatures and salinities deduced from the proxy data.

To facilitate the work with different data sets and time slices, SCINNA allows the employment of (1) arbitrarily shaped basins, taking into account topographic variations due to sea level changes and glaciation/deglaciation processes; (2) any T and S initialization fields; (3) arbitrary T, S, ice, and wind distributions for forcing the model; (4) arbitrary T and S restoring data; and (5) a simple prognostic sea ice model instead of a fixed ice cover.

SCINNA is a 3–D prognostic ocean general circulation model. It has been developed on the basis of the modular ocean model [*Pacanowski et al.*, 1993], the newly built version of the well–known Princeton circulation model [*Bryan*, 1969; *Cox*, 1984].

Being appropriate for modeling motions on a rotating sphere, SCINNA is written in 3–D spherical coordinates (refer to the appendix for an explanation of symbols and definitions). It uses the set of primitive equations, comprising conservation of momentum:

$$u_t = -\mathcal{L}u + fv + \frac{uv\tan\phi}{a} - \mathcal{P}_\lambda + \mathcal{D}^u, \quad (1)$$

$$v_t = -\mathcal{L}v - fu - \frac{uu\tan\phi}{a} - \mathcal{P}_\phi + \mathcal{D}^v, \quad (2)$$

$$p(z) = p_{\mathrm{surf}} + g\int_z^0 \rho\, dz, \quad (3)$$

conservation of mass (continuity equation):

$$w_z + \frac{1}{a\cos\phi}[u_\lambda + (v\cos\phi)_\phi] = 0, \quad (4)$$

conservation of heat and salt:

$$T_t = -\mathcal{L}T + \mathcal{C}^T + \mathcal{R}^T, \quad (5)$$
$$S_t = -\mathcal{L}S + \mathcal{C}^S + \mathcal{R}^S, \quad (6)$$

and a nonlinear equation of state (the complete writeout may be found in the appendix):

$$\rho = \rho(T, S, z). \quad (7)$$

At the lateral boundaries the no–slip condition (the fluid adheres to the walls) and no–flux conditions (no heat and salt fluxes across the walls) are applied:

$$u, v, T_n, S_n = 0. \quad (8)$$

The surface boundary conditions take into account the momentum transfer by winds:

$$\rho_0 A_{MV}(u_z, v_z) = \tau^\lambda, \tau^\phi, \quad (9)$$

and the fluxes of heat and freshwater:

$$A_{TV}(T_z, S_z) \propto \text{surface heat and freshwater fluxes.} \quad (10)$$

For eliminating external gravity waves, which require very short time steps and very long computing time, the rigid–lid condition (no vertical motions at the surface) is employed:

$$w = 0. \quad (11)$$

At the bottom the momentum flux is given by bottom friction:

$$\rho_0 A_{MV}(u_z, v_z) = \tau_B^\lambda, \tau_B^\phi, \quad (12)$$

and the tracer fluxes are kept zero, as it is the case for the lateral boundaries:

$$T_z, S_z = 0. \quad (13)$$

The boundary condition for vertical velocity,

$$w = -\frac{u}{a\cos\phi}H_\lambda - \frac{v}{a}H_\phi, \quad (14)$$

which ensures that the fluid follows bottom slopes, is automatically in effect because of the used discretization scheme.

For discretization the Arakawa–B–grid is employed, with a half grid distance's shift between T-S points and u-v points (see Figure 4).

For integration in time the leap–frog scheme is used, calculating the model's new state at a given time step n from the state of two steps previous $(n-2)$ and the time derivatives of the previous one $(n-1)$, or, symbolically (see Figure 5).

Numerous experiments based on the modern state of the northern North Atlantic have revealed a very high sensitivity of the model to even small changes in the forcing fields. Variations of T, S, and ice edge position within ranges comparable to their respective paleoreconstruction error estimates can alter the model's state significantly [*Keir et al.*, 1993]. This is particularly the case with respect to the combined influences of surface salinity and ice cover. For example, salinity changes of $1–2^0/_{00}$ can strengthen, cut off, or even reverse the East Greenland Current. Conversely, the wind's influence is less important, since the thermohaline forcing is dominating the circulation system. The model's response to forcing changes is very fast: it takes only a couple of decades to adjust. Rapid changes of this timescale in the real ocean have been recognized from high–resolution stratigraphy of the sedimentary record, so this seems to realistic.

The sensitivity experiments also uncovered inconsistencies and ambiguities in the climatological temperature and salinity data sets [*Levitus*, 1982] for the northernmost modern Atlantic. By incorporation of data representing the northern Atlantic's typical conditions much better [*Dietrich*, 1969], these contradictions can be avoided. For example, the East Greenland Current is not present in the *Levitus*, [1982], but in the *Dietrich*, [1969] data. Driven by consistent data, SCINNA reproduces the modern circulation patterns and water mass distributions well.

Because of the uncertainties and spatial limitations of available paleoreconstructions, inconsistencies are an inseparable property of paleotemperatures and paleosalinities. SCINNA helps to filter out the consistent features and calculate the corresponding circulation. For 18,000 B.P., first experiments have been made using the CLIMAP summer temperatures [*CLIMAP Project Members*, 1976] in combination with a superposition (D. Seidov, personal communication, 1993) of salinity reconstructions for this time slice.

SENNA

SENNA is a large–scale dynamic three–dimensional sedimentation model for the northern North Atlantic. It basically consists of two coupled models, the first one modeling the three-dimensional sediment transport in the water column [*Zanke*, 1977; *Bitzer and Pflug*, 1990; *McCave and Gross*, 1991], the second simulating the two–dimensional processes near the bottom in a layer 1 centimeter thick [*Zanke*, 1978; *Puls*, 1981; *Sündermann and Klöcker*, 1983]. These two models are coupled by the vertical exchange of suspended sediment (Figure 6). SENNA is driven by temperature, salinity, and velocity fields derived from experiments with ocean circulation models.

Although the topography is represented as a structure of stairs in the 3–D model, this can be neglected because the coupled bottom layer is kept parallel to the newly computed bottom shape at any time. In this way,

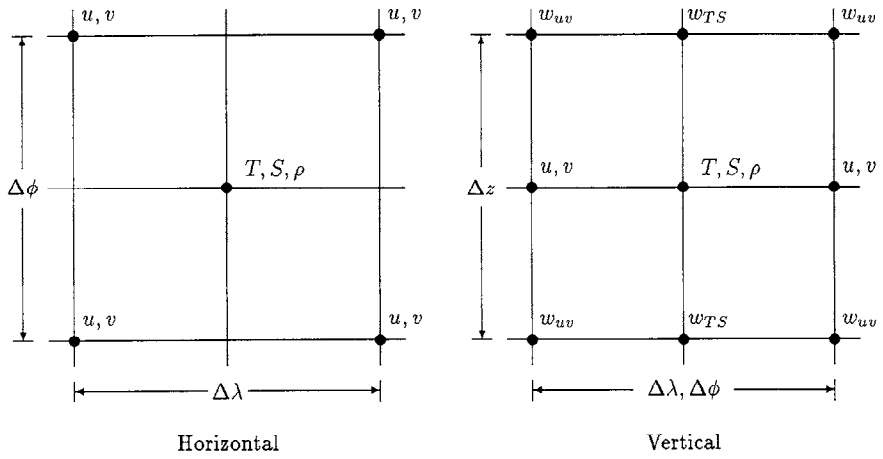

Figure 4. Spatial discretization of SCINNA.

a realistic modeling of processes parallel to the bottom slopes is possible.

A detachment of the flow from the stairs of the bottom topography in the 3–D model is only possible with turbulence where the bottom slope is greater than 5 deg [*Puls*, 1981]. This bottom slope in flow direction is not reached in the model (maximum $\leq$ 2.65 deg).

The structure of the model physics is simple so as to be able to run long time simulations. It is possible to model sediment dynamics based on terrigenous and biogenic sediment entry within a reasonable computer time. At the same time it is important to be able to resuspend and redeposit sediments that already have been deposited.

The 3–D model essentially contains the 3–D sediment transport equation

$$C_t = -\mathcal{L}C + \mathcal{S}, \tag{15}$$

and the 2–D model is based on the 2–D sediment transport equation:

$$C_t = -\mathcal{L}_H C + \mathcal{S}. \tag{16}$$

The lateral boundaries are closed as for SCINNA.

In the 3–D model the lateral entry of sediments and also the entry of particles, which come from melting icebergs into the upper part of water column, are taken into account.

At the lateral and the surface boundaries positive sediment sources for the sediment entry and negative sediment sources for the sediment sinks are prescribed at the boundaries. The mass of sediments can thus be reduced or increased within the model. These changes of the total mass of sediment in the water column are also envoked by erosion, redistribution, and deposition.

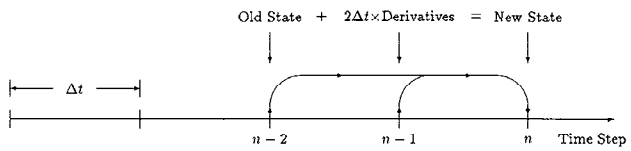

Figure 5. Leap frog time stepping.

The particles that are suspended in the water column are carried by the currents [*Bitzer and Pflug*, 1989]. In addition to the vertical velocity of the surrounding water, the sink velocity of particles has to be considered. This velocity depends on grain size, density and kinematic viscosity of the surrounding water as well as on particle density, on form factor, and on sedimentological grain diameter [*Zanke*, 1977; *McCave and Cross*, 1991]:

$$w_{\text{sink}} = w_{\text{sink}}(\nu, gs, D^*, \rho, \rho_{\text{sed}}, FF, g) \tag{17}$$

In the 2–D bottom model, near bottom processes are considered. These include erosion, transport and deposition which depend on critical velocities, that is, critical erosion and suspension velocity, and on the sediment contents of the one centimeter thick bottom layer, as well as on grain size, form factor etc. [*Zanke*, 1977, 1978; *McCave*, 1984].

$$u_{S\text{crit}} = u_{S\text{crit}}(u_{\text{bot}}, v_{\text{bot}}, \nu, gs, D^*, \rho, \rho_{\text{sed}}, FF, g) \tag{18}$$

$$v_{S\text{crit}} = v_{S\text{crit}}(u_{\text{bot}}, v_{\text{bot}}, \nu, gs, D^*, \rho, \rho_{\text{sed}}, FF, g) \tag{19}$$

$$u_{B\text{crit}} = u_{B\text{crit}}(u_{\text{bot}}, v_{\text{bot}}, \nu, gs, \rho, \rho_{\text{sed}}) \tag{20}$$

$$v_{B\text{crit}} = v_{B\text{crit}}(u_{\text{bot}}, v_{\text{bot}}, \nu, gs, \rho, \rho_{\text{sed}}) \tag{21}$$

The near–bottom velocities result from a reduction of the velocity of the layer most proximal to the bottom [*Zanke*, 1978; *Sündermann*, 1983]. Also, the bottom slope in direction of the bed load and the suspension load transport [*Krohn*, 1975; *Puls*, 1981] is taken into account. An upward directed bottom slope increases the critical velocities, and at the same time reduces the erosion rate and vice versa. For example, if the velocity decreases or if the depth grows, in the direction of particle flow, the sedimentation material is deposited.

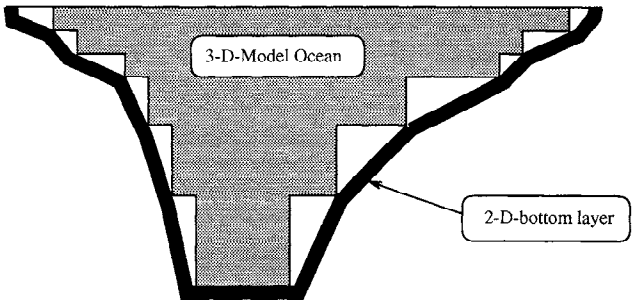

Figure 6. The 3–D and 2–D coupling in SENNA and PATRINNA.

The same process takes place if there is an upward directed bottom slope and when the two critical velocities increase.

For the 2–D model the change of bottom topography is calculated from the modeled changes of the sediment contents in the one centimeter thick (near) bottom layer [*Puls*, 1981; *Sündermann*, 1983].

In order to simplify calculations, both combined models are based on a homogeneous grain mixture of a medium–sized sedimentological grain diameter [*Sündermann*, 1983].

Since elementary relations of sediment movements usually depend on mechanical processes, and because of the mostly unknown influence of biological factors on waters, the following effects are not considered: (1) the coagulation by microorganisms; (2) the roughness of sediments changes due to organical films; (3) flocculation effects of organic sediments and mixture with sands; and (4) cohesion. The motion of the sea in the upper layers is also neglected.

PATRINNA

PATRINNA works out the main drifting patterns as well as the residence time of particles or sediment plumes/clouds in different areas or basins, respectively. It consists as SENNA of two coupled models: the 3–D model calculates the 3–D drift in the water column. The 2–D model considers the drift parallel to the seafloor. Both models were developed for tracing particles.

PATRINNA uses the same driving fields as SENNA, together with the topography changes computed by the latter. As in SENNA, particles are considered to move horizontally with the prescibed horizontal velocity [*Bitzer and Pflug*, 1989].

From the horizontal velocities the vertical velocity is calculated by means of the continuity equation. The sink velocity is additionally superimposed. This velocity originates from observations as well as from empirical equations [*Zanke*, 1977; *Gibbs*, 1985].

From a particle's given position and the velocity field at this point the new position is calculated by

$$\begin{aligned} \lambda_{\text{new}} &= \lambda_{\text{old}} + \frac{u}{a\cos\phi}\Delta t \\ \phi_{\text{new}} &= \phi_{\text{old}} + \frac{v}{a}\Delta t \\ z_{\text{new}} &= z_{\text{old}} + w\Delta t. \end{aligned} \tag{22}$$

PATRINNA uses the reduced bottom velocity of SENNA in the bottom layer [*Zanke*, 1978; *Sündermann*, 1983]. The bottom slope is considered in the same way as in SENNA. Special attention is given to the reconnaissance of the mean sediment drifts and to the residence time of particles and particle clouds in different regions.

Interconnection of the Models

SCINNA is initialized with temperatures and salinities from measurements and/or paleoreconstructions. With application of surface wind, temperature, ice, and salinity distributions the time integration proceeds until the rate of change of the model's state is small (lower than 1 ° C respectively 0.1 ‰ per 500 years) compared to the rates indicated by proxy data (about 3 °–5 ° C respectively 1 ‰ per 500 years) (Figure 7a). At this point, the temperatures, salinities, and velocities are transferred as initial fields to SENNA and PATRINNA. These in turn calculate the sedimentation processes for the desired time interval (Figure 7b).

Because the topographic changes due to sedimentation/erosion processes are negligible compared to SCINNAs vertical resolution, a coupling from SENNA back to SCINNA is not neccesary.

Results

Here the results of two experiments will be discussed, the first (M) was run to model the modern situation, the second (LGM) gives first results for the LGM 18,000 years B.P.

Experiment M used the topography shown in Figure 3 and was initialized with the winter temperatures and salinities of *Levitus* [1982] and *Dietrich* [1969]. These data sets were used also for restoring and haline forcing (Figure 8a and 8b). For thermal forcing, the original temperatures were replaced by -1.9 ° C below the typical winter ice cover (Figure 8a). The wind was taken from the January data of *Hellerman and Rosenstein* [1983].

To account for glacial sea level change, the overall depth was reduced by 100 m in the LGM experiment, accompanied by selectively clipping off all regions shallower than 200 m, thereby simulating shelf glaciation (Figure 9). With the exception of the Bear Island Trough this procedure cuts off the Barents Sea, and reduces the cross sectional areas of the straits between Greenland, Iceland, and Scotland. Initialization and wind forcing were identical to those of experiment M. For thermal forcing and ice cover the CLIMAP summer reconstruction was employed (Figure 10a), whereas for haline forcing a superposition (D. Seidov, personal communication, 1993) of salinity reconstructions by *Duplessy et al.* [1991] and M. Sarnthein et al. (personal communication, 1993) (Figure 10b) was used. Combining these two data sets is, of course, inconsistent, since the salinities were calculated with an ice–free Greenland and Norwegian Sea, in contrast to the ice cover recon-

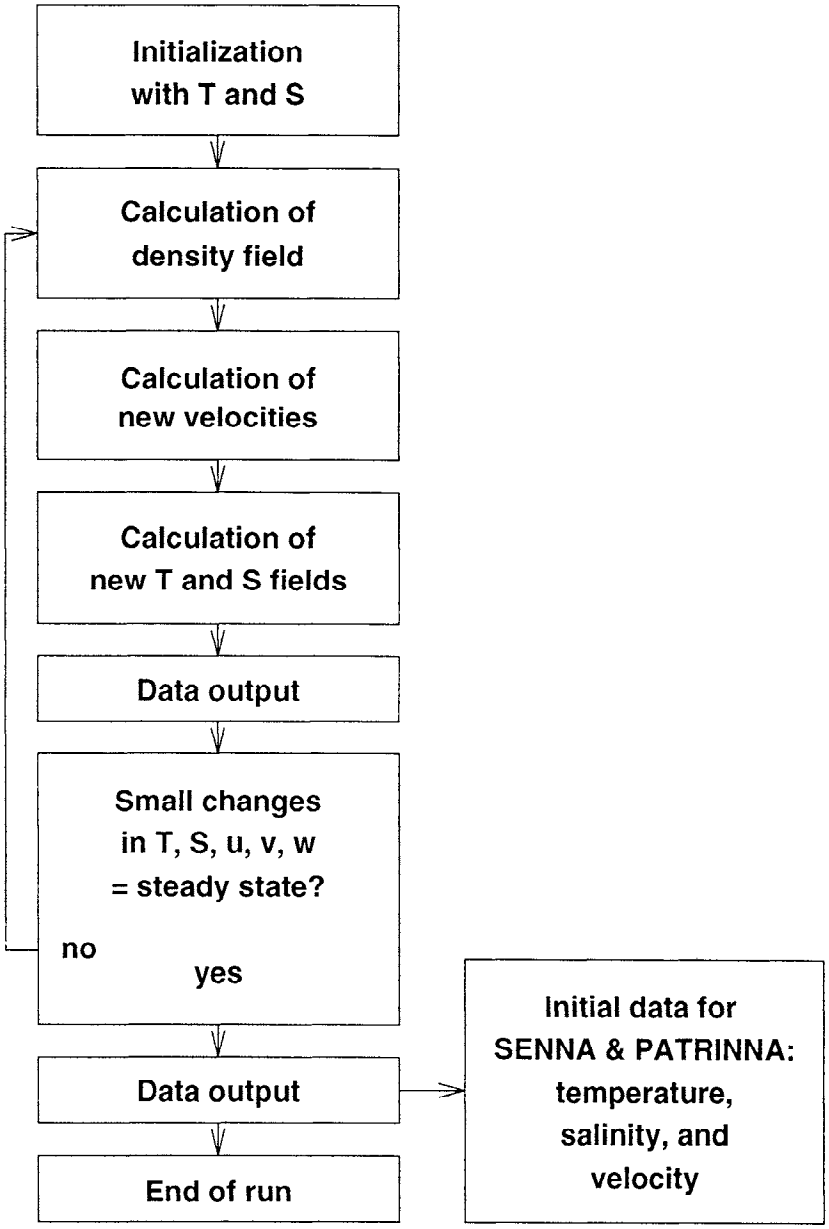

Figure 7. Integration schemes and coupling of SCINNA, SENNA, and PATRINNA.

structed by CLIMAP. We ran several experiments using different ice–free areas in the Greenland and Norwegian Seas. However, because of the very high salinity reconstruced for this region the density field and the circulation showed only minor changes. We therefore present only the results from the ice–covered model run. On the other hand, these surface forcing data are by no means consistent with the modern 3–D distributions of temperature and salinitiy, so that the latter cannot be used for restoring. However, recent 3–D paleoreconstructions [*Sarnthein et al.*, 1993] have not yet been prepared for model use, so this experiment was run without restoring.

Our principle goal is to compare the modern with the LGM state, in this special case modern and LGM winter. However, our knowledge about the past is still very limited. Therefore we rather must attempt to find out the characteristics of past time slices and start with the data being at hand. The LGM winter reconstructions are very poor at the moment, so we first tried to model the summer situation derived from the available proxy data.

With the modern forcing, SCINNA produces most prominent circulation patterns as they are known for today. Figure 11a shows the resulting stream function, that is, the vertically integrated mass transport. Val-

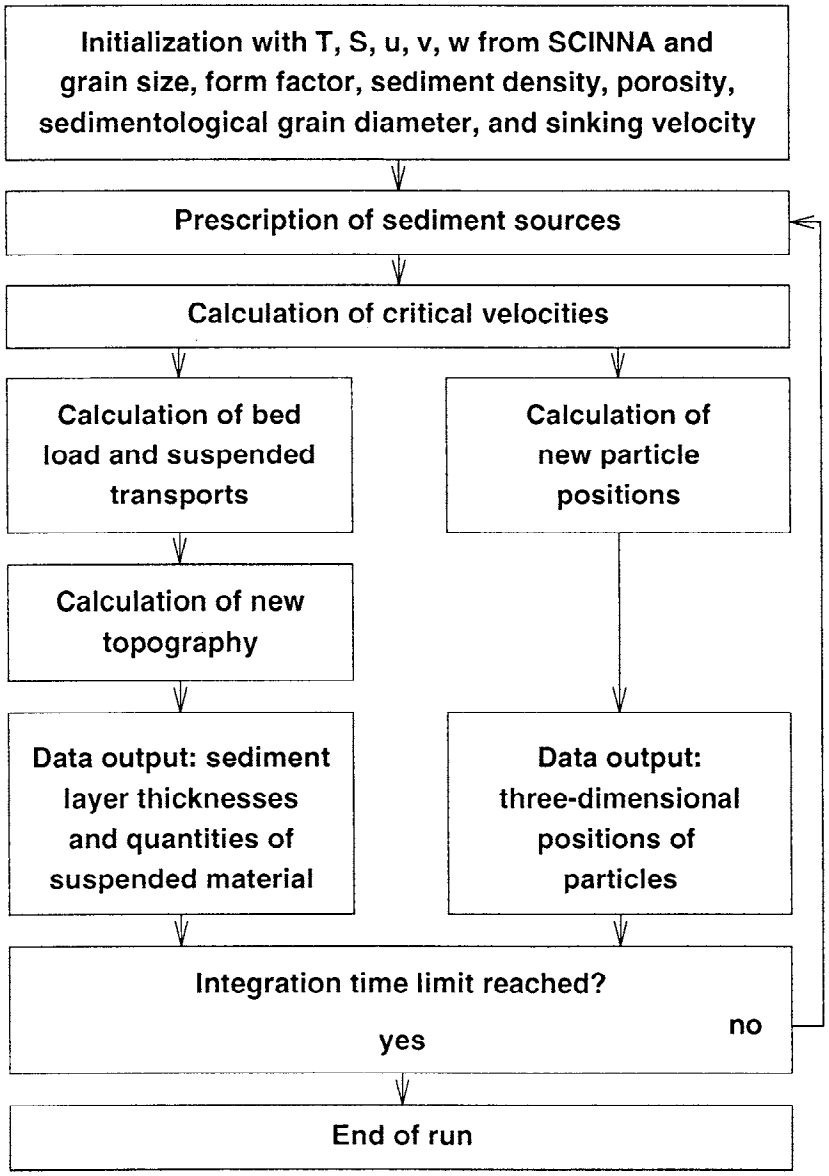

Figure 7. (continued)

ues are given in sverdrups (1 Sv = 10^6 m^3s^{-1}), negative for cyclonal, positive for anticyclonal motion. (For the deepwater flows, refer to the PATRINNA results shown below.) The subtropical and subpolar gyres are apparent, presenting a schematic Gulf Stream and Labrador Current at their respective western boundaries. The two gyres are separated by the North Atlantic Current directed northeast from Newfoundland to Ireland. It's continuation, the Norwegen Current, enters the Norwegian Sea with a transport of approximately 1.5 Sv. This inflow is balanced by the combined outflows of the East Greenland and East Iceland Currents.

In the LGM experiment the absence of lateral restoring reduces the transports of the subtropical and subpolar gyres, and the Gulf Stream and the Labrador Current are notably less sharp than in the modern run. The gyres' shapes, however, remain essentially the same (Figure 11b).

The main differences occur in the Greenland–Norwegian Seas and at the ridges between Greenland, Iceland, and Scotland. The combination of temperatures around freezing point (Figure 10a) and high salinity at the surface (Figure 10b) causes an intensification of the cyclonal circulation to values of about 6 Sv, whereas the flows over the ridges are reduced to approximately 1 Sv because of reduced sea level. Both results are subject to further investigation, since the actual ice extent at 18,000 years B.P. is not known exactly. As already mentioned, there might have been an ice-free region north of Iceland, which slows down the cyclonal motion in the basin to some extent due to higher surface temperatures. Further on, the transports over the ridges could

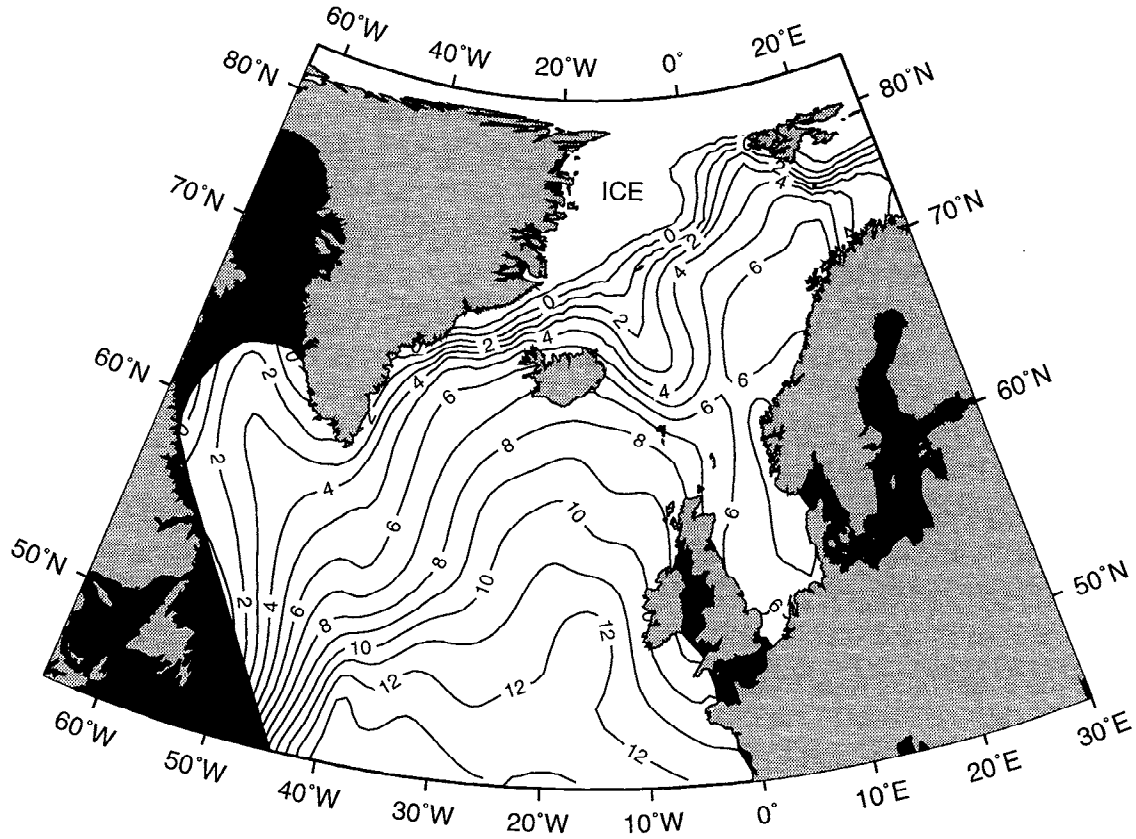

Figure 8a. Modern winter surface temperature, in degrees celsius, plus mean winter ice cover.

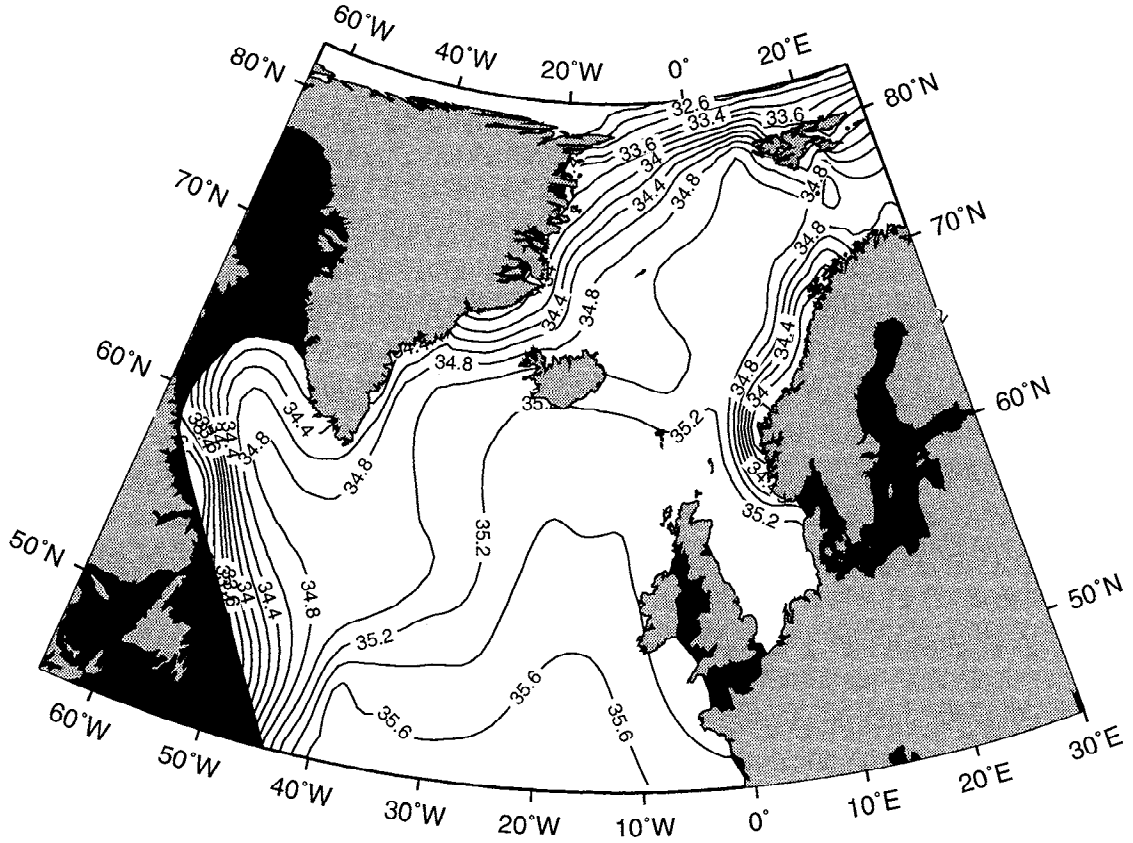

Figure 8b. Modern winter surface salinity in in parts per thousand.

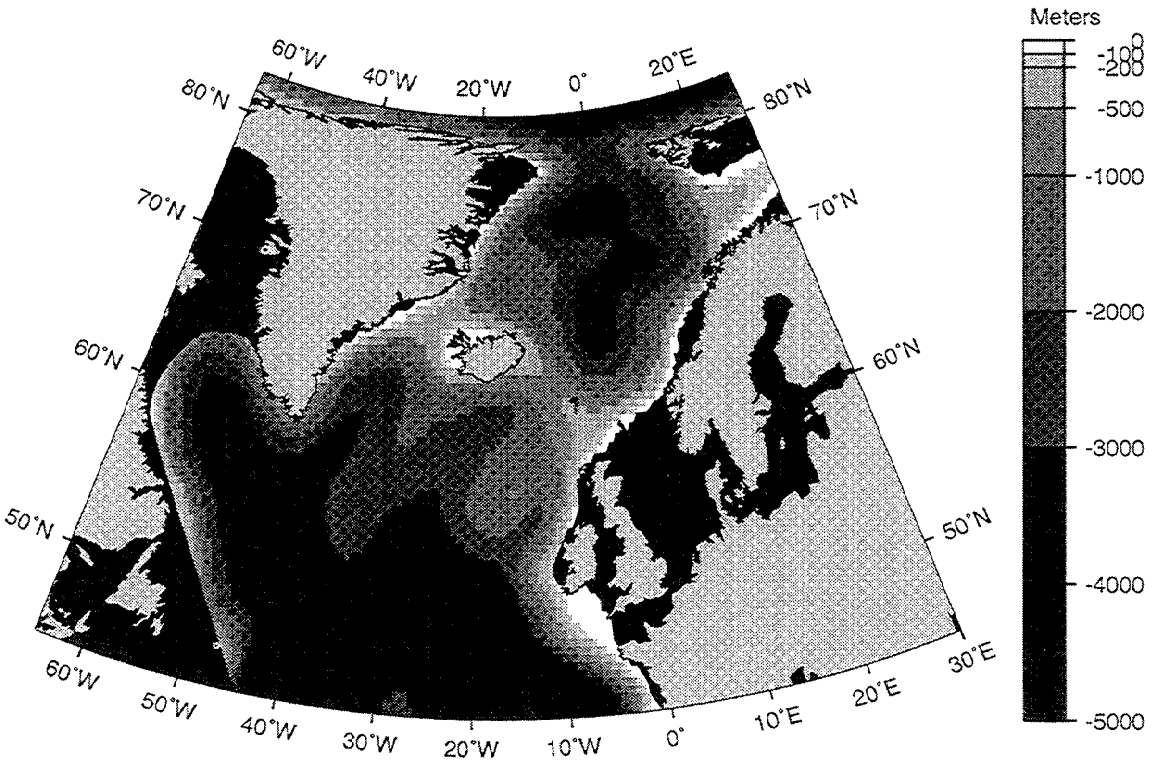

Figure 9. Model topography for the last glacial maximum experiments.

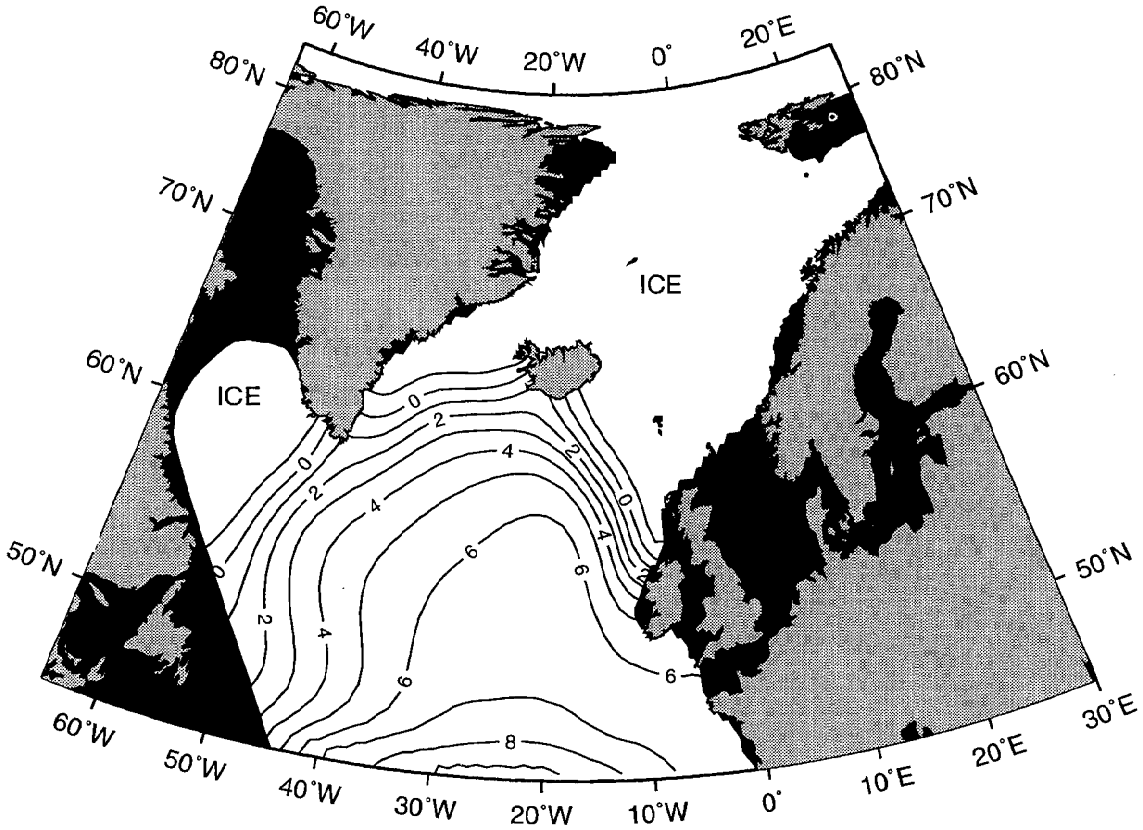

Figure 10a. CLIMAP summer surface temperature for the last glacial maximum, in degrees celsius.

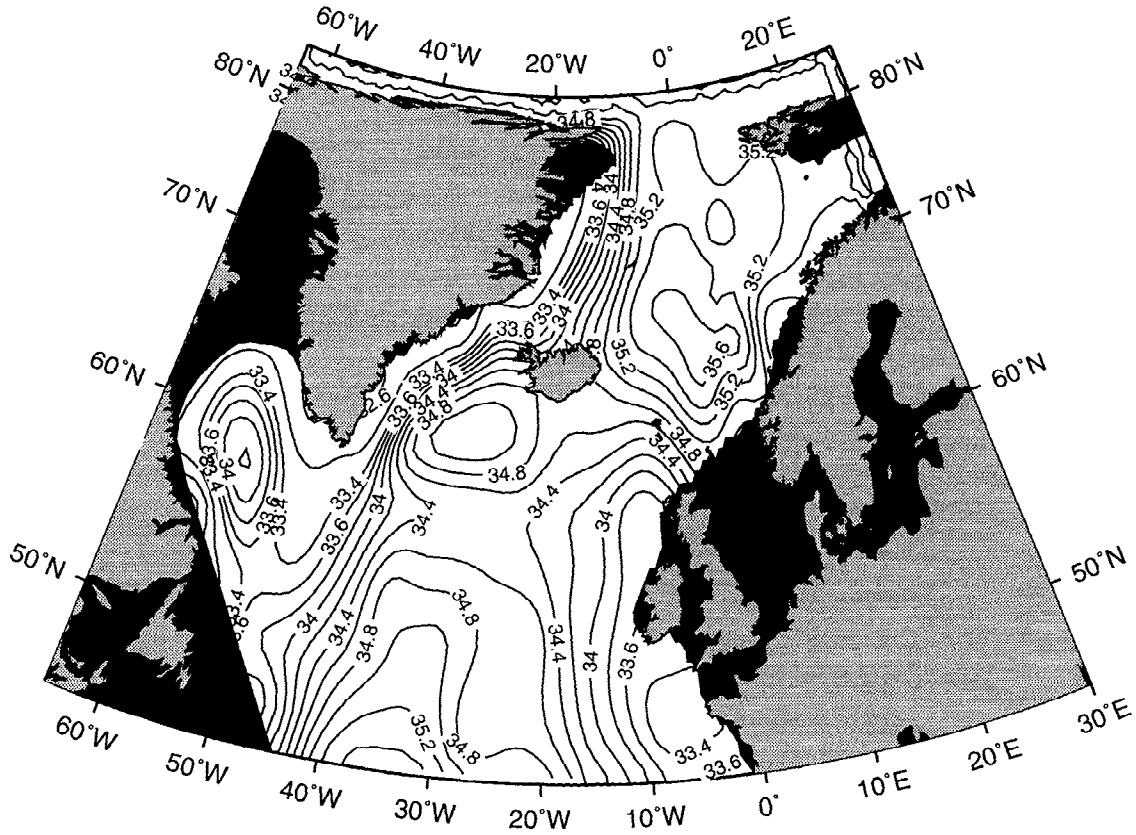

Figure 10b. Summer surface salinity for the last glacial maximum in parts per thousand.

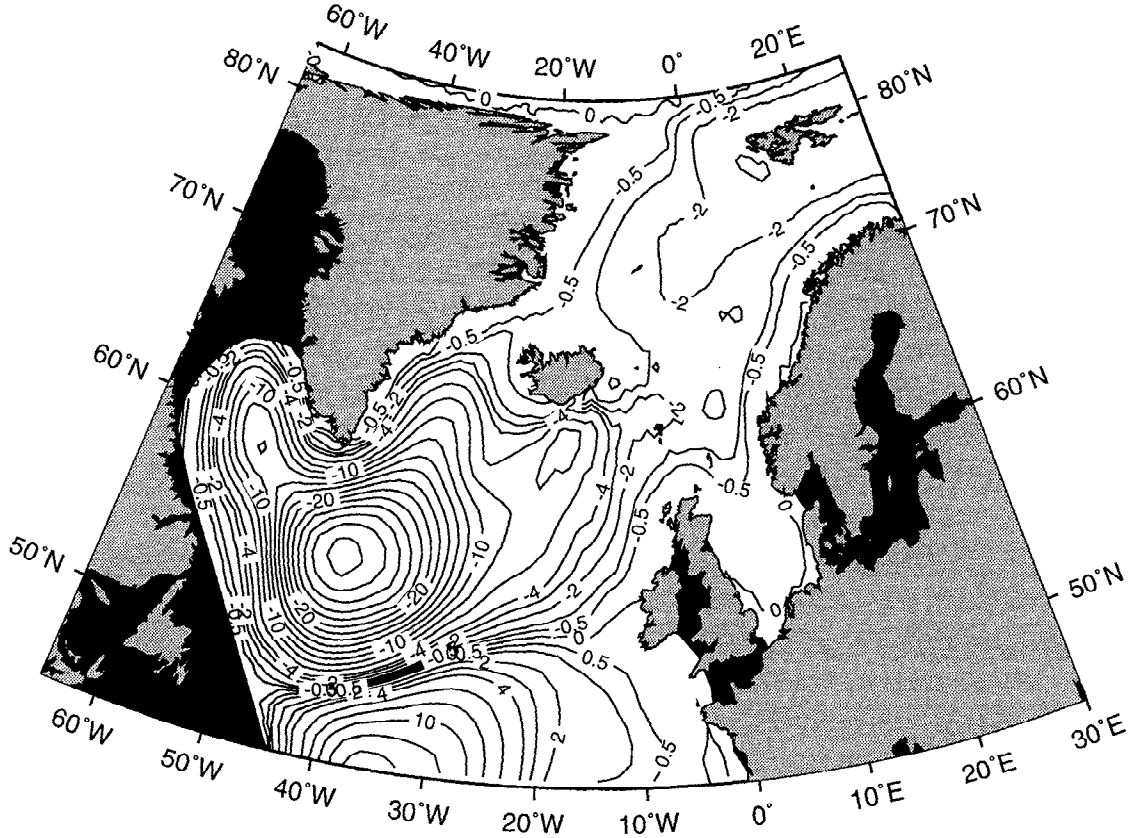

Figure 11a. Modern circulation pattern, mass transport in sverdrups.

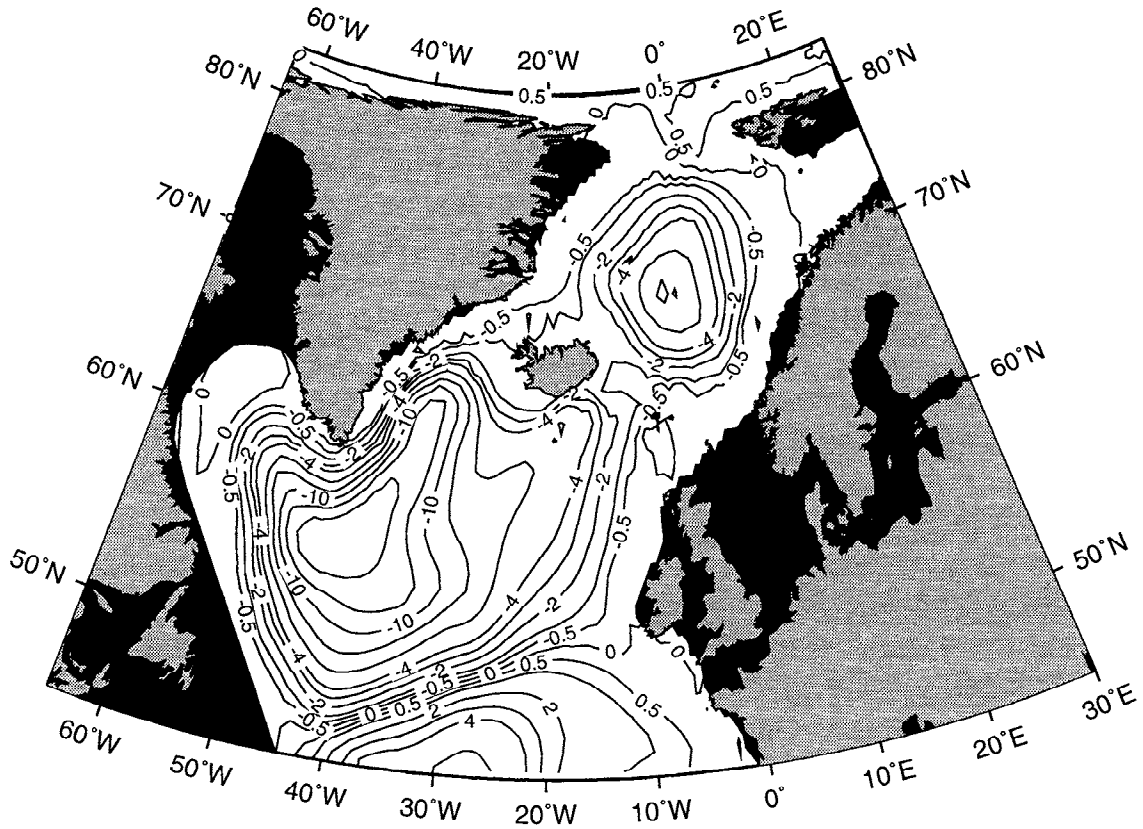

Figure 11b. Circulation resulting from the last glacial maximum forcing, mass transport in sverdrups.

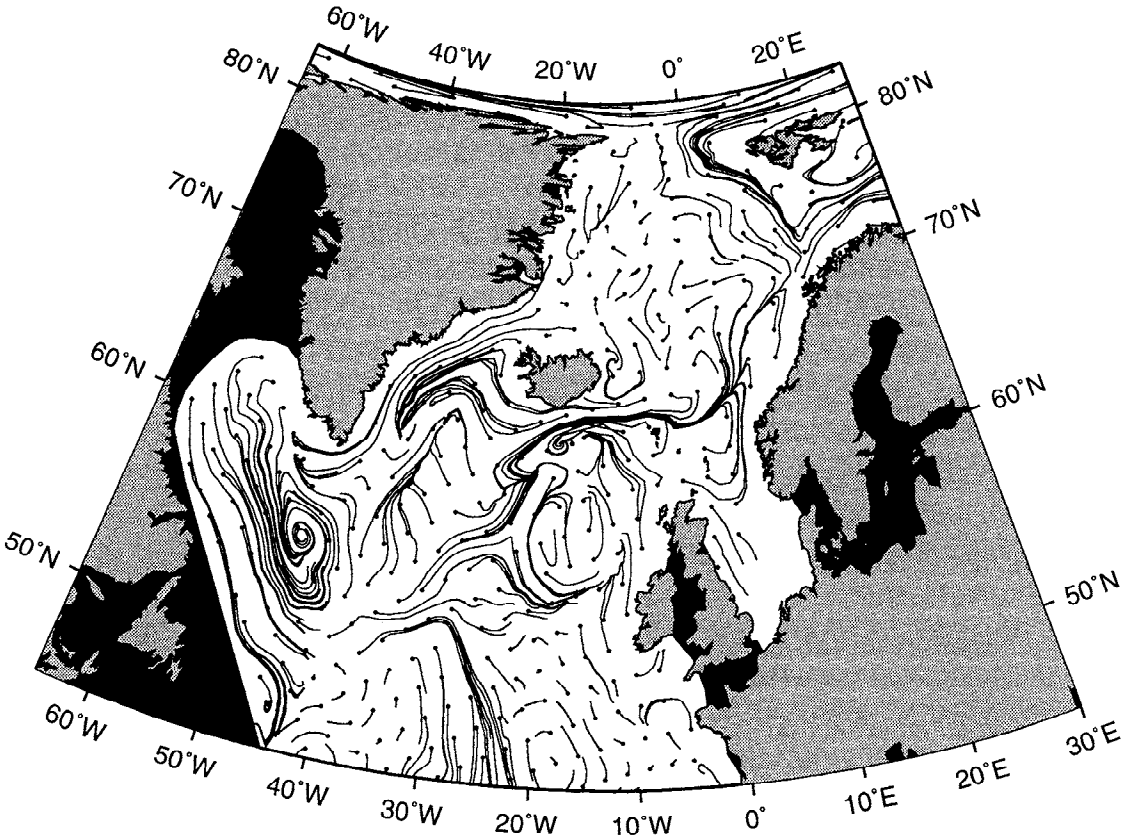

Figure 12a. Modern particle traces in the bottom layer, 10 years transport.

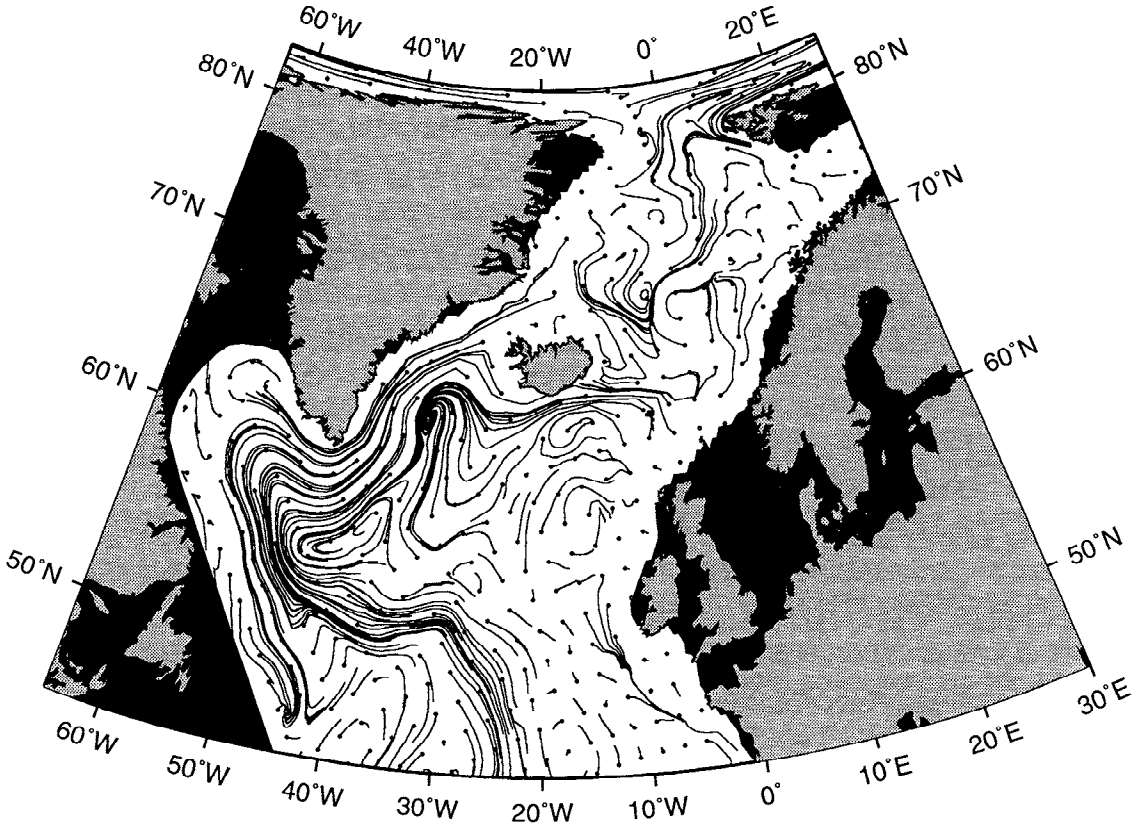

Figure 12b. LGM particle traces in the bottom layer, 10 years transport.

have been cut off completely by a suspected ice barrier between Greenland and Scotland.

The bottom currents of both experiments will be compared along with the resulting sediment drifts modeled by SENNA and PATRINNA:

The four experiments (two with SENNA, two with PATRINNA) are initialized with the output data of SCINNA. These data sets contain the 3–D fields of temperature and salinity and the 3–D velocity field. For both time slices, M and LGM, the sediment properties (sediment sources, sinking velocity ($0.05\,\mathrm{cm\,s^{-1}} = 43.2\,\mathrm{m\,d^{-1}}$), density of sediment, grain size, and sedimentological grain diameter, form factor of sediment particles and sediment porosity) are the same in order to simplify comparison of both experiments. In addition, the critical velocities for suspended load transport and bed load transport have been set to the same magnitudes in both cases.

The two experiments with PATRINNA show the movement of particles parallel to the 2–D bottom layer (Figure 12a and 12b) within a period of 10 years. In both model runs, 495 particles are started which are equally distributed over the model area.

In these experiments the magnitudes of the critical velocities for bedload and suspended transports are reduced in order to stay below the magnitudes of the horizontal velocities in the bottom layer. So doing simplifies working out the main sediment motions near the bottom. Although *Zanke* [1978] and Hjulstrom suggest values for critical velocities, their magnitudes cannot be used because they are developed for shallow water conditions, rather than for deep–sea regions. In shallow seas, near bottom velocitis are typically around $10\,\mathrm{cm\,s^{-1}}$. In the deep basins of the models there are regions with only small values of about $1\,\mathrm{cm\,s^{-1}}$. In all other parts in the deep sea they are below $0.01\,\mathrm{cm\,s^{-1}}$.

Figure 11a shows the main currents according to the actual state of knowledge, for example, the Labrador, East Greenland, Irminger, and Norwegian Currents. These circulation patterns also appear during the last glacial maximum, but shifted to other regions (Figure 12b).

The two experiments with SENNA show the amount of eroded, transported and finally deposited material (Figure 13a and 13b). Both model runs enclose a period of 2000 years. It is worth noting that both experiments use the same initialization for the sediment physics, but different initialization for the ocean physics (temperature, salinity and velocity), which is provided by the output of SCINNA's model runs.

Because the model input concerning the 3–D distribution of sediment sources and sinks has not yet been completed, we assume for these first experiments that (1) sediment input only occurs in the uppermost layer; (2) sediments are available on the seafloor; and (3) lateral input is not provided. The prescribed flux is about $1.0\times10^{-13}\,\mathrm{g\,cm^{-2}s^{-1}}$ ($= 0.0864\,\mathrm{mg\,m^{-2}d^{-1}}$).

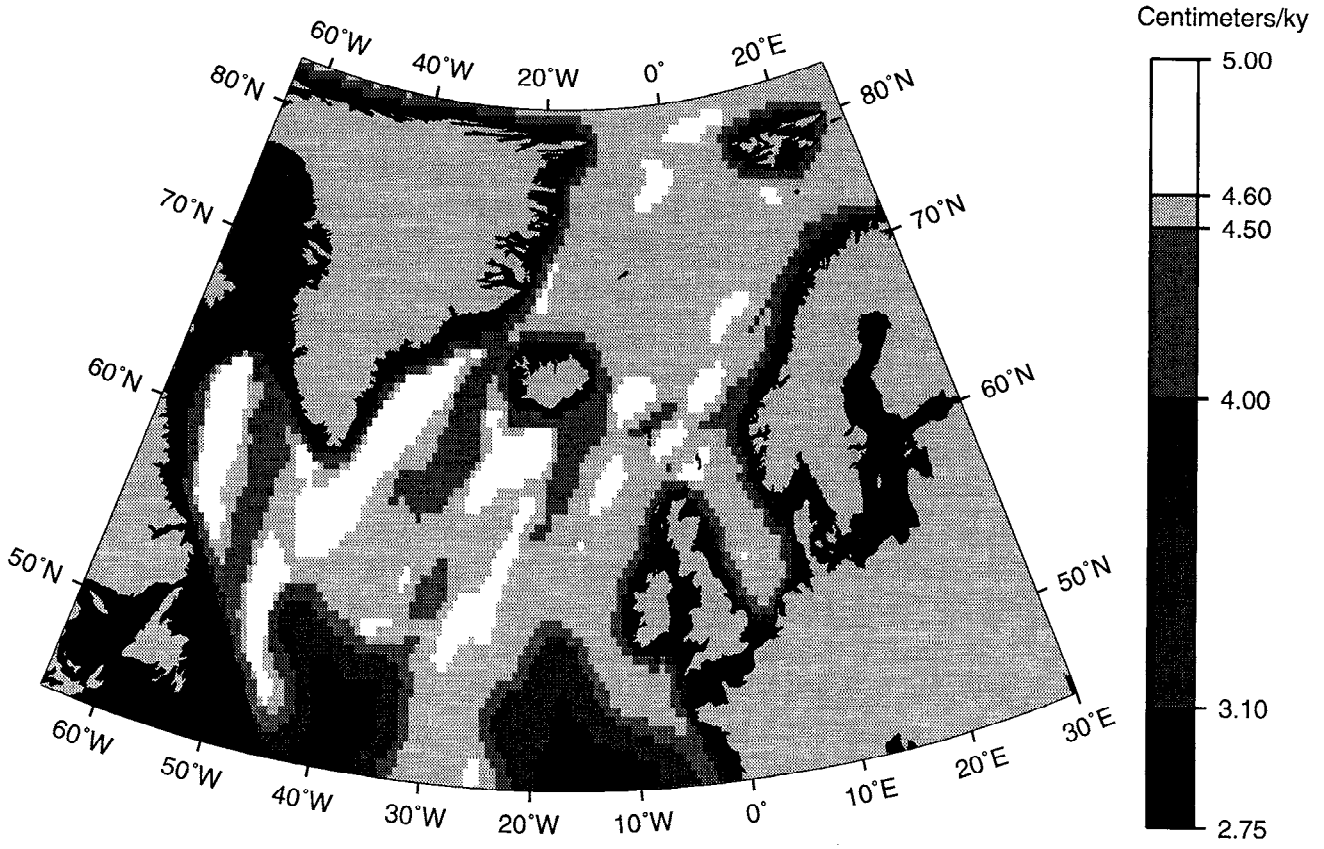

Figure 13a. Modern sediment accumulation after 2000 years.

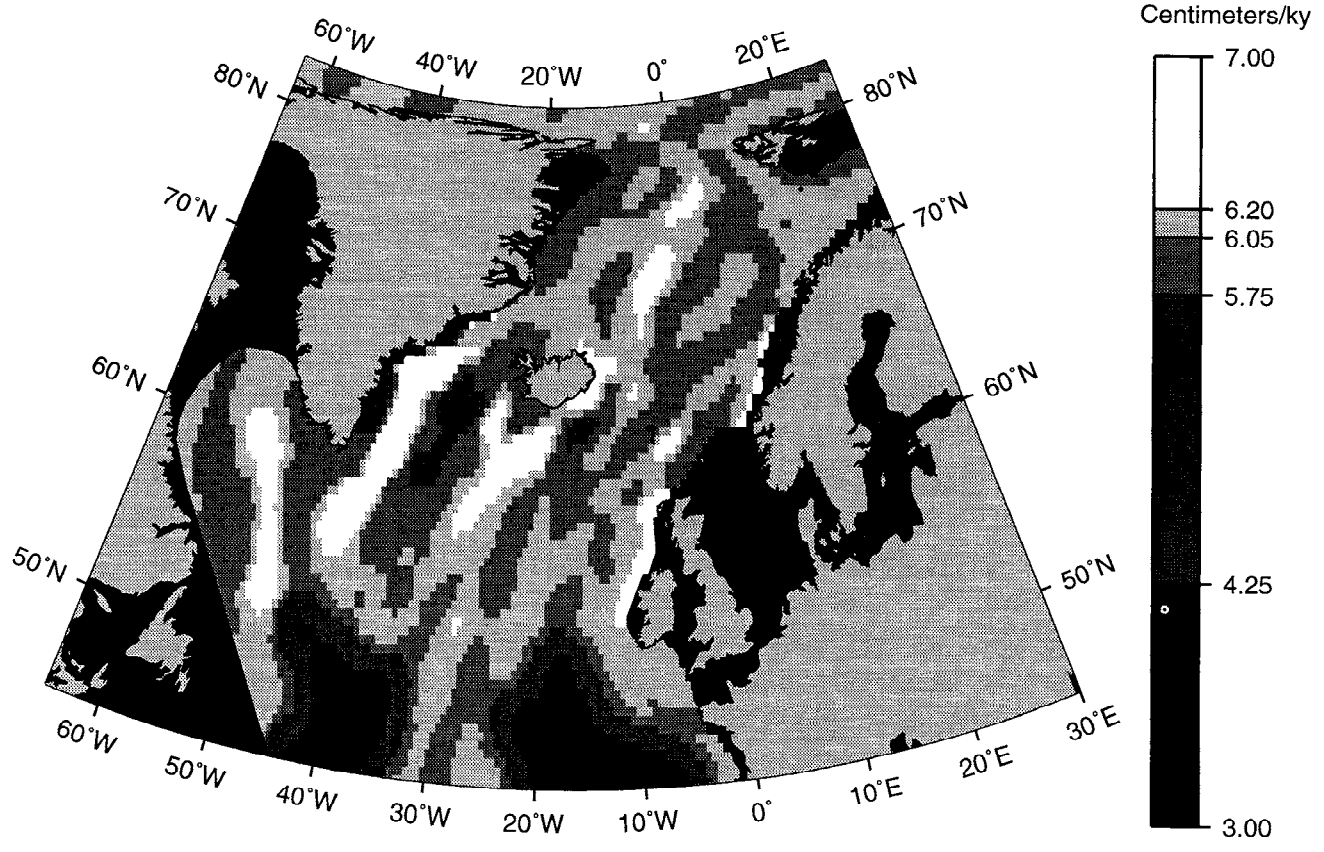

Figure 13b. LGM sediment accumulation after 2000 years.

This value is lower compared to most values known from the literature [*Miller et al.*, 1977; *Honjo*, 1990]. In addition, the erosion rate, which depends on the bottom velocity, is reduced. These modifications have been introduced due to the fact that the most sensitive parameters in the model equations are firstly this erosion rate and secondly the critical velocities for bed load transport and supension load transport. In this way no small deep gaps in the bottom topography are produced in small areas with artificial high velocities.

The resulting sediment distribution patterns from SENNA extend mainly in the NE-SW direction. Most of the large sediment drifts in the NNA can be recognized as high accumulation areas, yielding up to 5 respectively 7 cm of sediments per 1000 years. Especially in the western and central part, the modeled high–accumulation areas fit well the distributions of the Gloria Drift, Eirik Drift, Bjorn Drift, and Hattar Drift (compare Figures 1 and 13a). Snorri Drift is shifted to the west. Only Gadar Drift east of the Reykjanes Ridge and and Feni Drift southeast of the Rockall Plateau are not adequately represented. This is probably due to small–scale topographic effects which can not be resolved by the model topography but influence the circulation pattern, and due to the neglection of lateral sediment input. In the LGM experiment (Figure 13b), Gloria Drift, Eirik Drift, and Bjorn Drift are high sediment accumulation areas again. The fit of Gadar Drift is much better compared to the modern case. The other sediment drifts yielded less sediment due to the different ocean circulation. This partly changing sediment supply is shown in the accumulation map adding both the modern and the LGM state (Figure 14) where we find continuous high–sediment supply for Gloria Drift, Eirik Drift, and Bjorn Drift.

The two southern regions of low sedimentation rate (darkly colored) are an artifact of the closed south boundary. With the restoring technique it is possible to simulate the missing inflow and outflow of sediment at this boundary in order to realistically prescribe the rest of the North Atlantic. This restoring can be done by prescibing the sediment sources and sinks at all closed boundaries to take into account the terrigenous sediment input.

Conclusions

Since sediment drifts in an oceanic basin develop together with ocean currents, a suitable modeling approach must take into account this strong dependence by coupling the processes of erosion, transport, and deposition of sediments to the oceanic circulation pattern. In this way our approach intends to base the sedimentation processes modeled by SENNA and PATRINNA

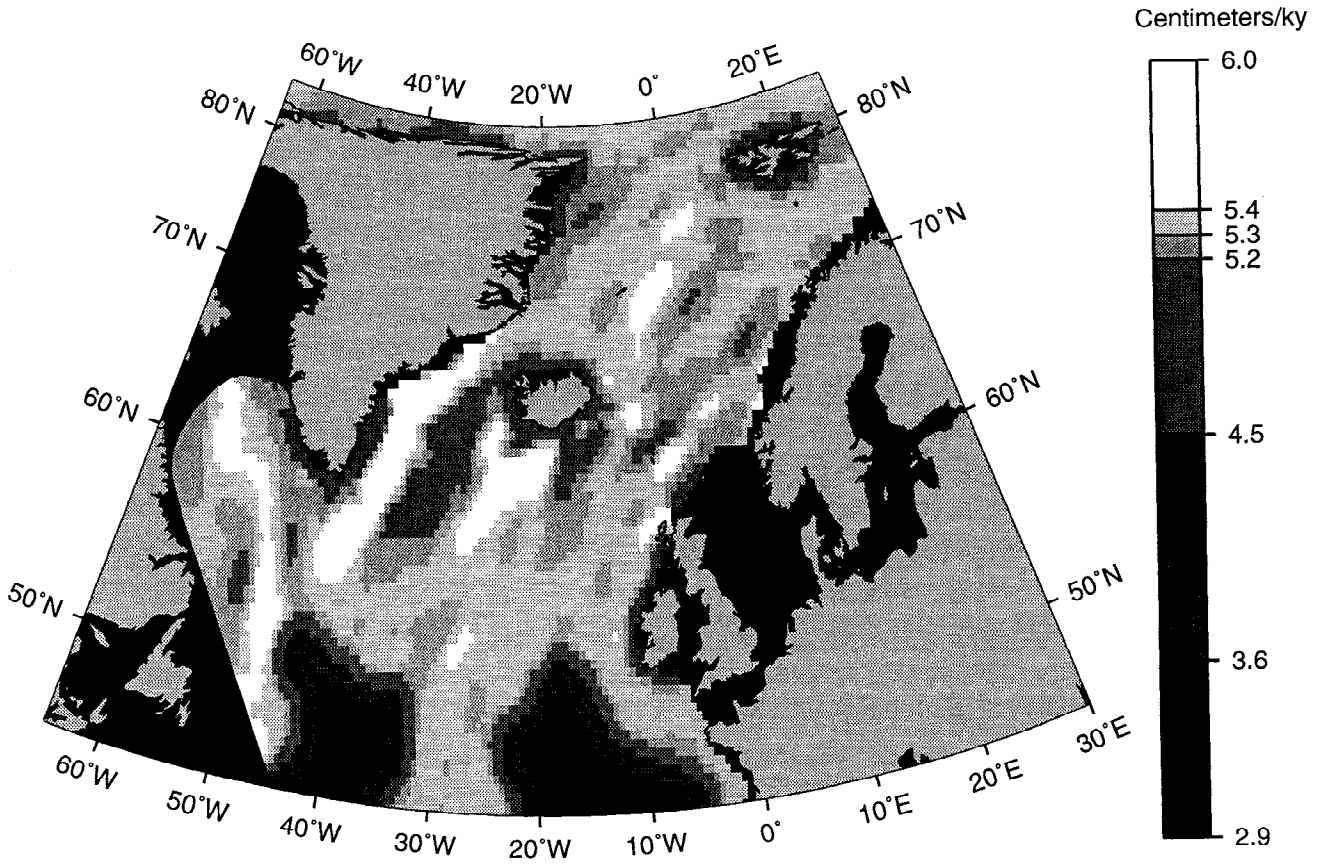

Figure 14. Modern plus LGM sediment accumulation after 2000 years.

on topography, temperatures, salinities, and current velocities of the NNA calculated by SCINNA.

From our model experiments we have clear evidence that (1) modeled and observed modern sediment drifts show very similar distribution patterns; (2) the three models and their coupling give reliable results for the modern case, and therefore this approach can be used for modeling the geologic past; (3) the general sedimentation patterns changed in in time in accordance with the changes in the NNA circulation due to climatic changes, if we compare the LGM and modern cases; and (4) some sediment drifts in the NNA yielded continuous sediment supply in the LGM and the modern case, especially in those areas where topography did strongly constrain the ocean currents.

At the present state it is possible to model the main sediment drifts of specially chosen time slices including the changes of topography. For this, different data sets of sediment sources and sinks are required. Additionally, we need more detailed informations about paleotemperatures, salinities, and ice cover. SCINNA requires these data for the surface and lateral boundary conditions. SENNA needs information about sediments transported by ice, which are suddenly set free when the ice melts. Moreover, the calculated data must be compared with core data and measurements of sediment traps. Throughout all these steps, it is necessary to improve the models continouosly. One of the next tasks will be to implement stratification and velocity shear dependent turbulence to vary the bottom velocities. With this technique it will be possible to model underwater sediment storms and sediment slides and slumps more realistically. In addition, other transport formulae are to be tested in SENNA for the modeling of sediment transports by deep–sea currents.

Table A1. Reference values of T, S, and ρ

k	T_k^0, °C	S_k^0, ‰	ρ_k^0, gcm^{-3}
1	13.4965263	32.75	1024.6883
2	13.4895577	32.75	1024.9119
3	13.4825610	32.75	1025.1353
4	13.4755362	32.75	1025.3584
5	8.4736287	35.15	1028.4758
6	8.4628420	35.15	1028.9283
7	8.4519207	35.15	1029.3799
8	5.9443101	34.90	1030.3609
9	4.4303652	34.90	1031.7045
10	3.9124148	34.75	1032.7904
11	2.9010129	34.75	1034.0563
12	2.8688735	34.75	1035.7548
13	2.8225733	34.80	1038.0375
14	2.7727705	34.80	1040.2573
15	2.7194480	34.80	1042.4537
16	2.6627227	34.80	1044.6271
17	2.5715099	34.80	1047.8446

Table A2. Coefficients $c_{k,n}$ of the Equation of State

k	$c_{k,1}$	$c_{k,2}$	$c_{k,3}$	$c_{k,4}$	$c_{k,5}$
	$c_{k,6}$	$c_{k,7}$	$c_{k,8}$	$c_{k,9}$	
1	-2.019687e-4	7.729232e-1	-4.913364e-6	-2.020104e-3	3.167594e-1
	3.602500e-8	3.770801e-3	3.600313e-5	1.609162e 0	
2	-2.028857e-4	7.725897e-1	-4.898396e-6	-2.015116e-3	3.160942e-1
	3.583541e-8	3.755316e-3	3.591824e-5	1.608385e 0	
3	-2.038018e-4	7.722565e-1	-4.883436e-6	-2.010123e-3	3.154241e-1
	3.564550e-8	3.739838e-3	3.583343e-5	1.607620e 0	
4	-2.047167e-4	7.719237e-1	-4.868485e-6	-2.005125e-3	3.147493e-1
	3.545527e-8	3.724369e-3	3.574869e-5	1.606869e 0	
5	-1.614386e-4	7.826868e-1	-5.279012e-6	-2.318765e-3	4.664893e-1
	4.415495e-8	4.584355e-3	4.312038e-5	1.509887e 0	
6	-1.635944e-4	7.819692e-1	-5.243779e-6	-2.307124e-3	4.496478e-1
	4.374243e-8	4.542186e-3	4.291617e-5	1.507958e 0	
7	-1.657448e-4	7.812532e-1	-5.208582e-6	-2.295472e-3	4.324421e-1
	4.332827e-8	4.500098e-3	4.271221e-5	1.506078e 0	
8	-1.427671e-4	7.857341e-1	-5.473062e-6	-2.479082e-3	3.130163e-1
	4.917646e-8	4.919470e-3	4.700753e-5	1.566492e 0	
9	-1.323861e-4	7.875783e-1	-5.587350e-6	-2.579612e-3	1.293001e-1
	5.230482e-8	5.064699e-3	4.937115e-5	1.592754e 0	
10	-1.326774e-4	7.868882e-1	-5.559262e-6	-2.587721e-3	-6.486547e-2
	5.262983e-8	5.028338e-3	4.973295e-5	1.607013e 0	

Table A2. (continued)

k	$c_{k,1}$	$c_{k,2}$	$c_{k,3}$	$c_{k,4}$	$c_{k,5}$
	$c_{k,6}$	$c_{k,7}$	$c_{k,8}$	$c_{k,9}$	
11	-1.279715e-4	7.875341e-1	-5.607799e-6	-2.648123e-3	-4.305191e-1
	5.445939e-8	5.044215e-3	5.113075e-5	1.623649e 0	
12	-1.375271e-4	7.846205e-1	-5.449187e-6	-2.594500e-3	-1.514955e 0
	5.259628e-8	4.823367e-3	5.015014e-5	1.615151e 0	
13	-1.502227e-4	7.807921e-1	-5.236764e-6	-2.522783e-3	-3.678225e 0
	5.003982e-8	4.530014e-3	4.884512e-5	1.601324e 0	
14	-1.625888e-4	7.769931e-1	-5.028772e-6	-2.451867e-3	-5.035793e 0
	4.747688e-8	4.245158e-3	4.755586e-5	1.592347e 0	
15	-1.747446e-4	7.732404e-1	-4.823038e-6	-2.381379e-3	-6.526288e 0
	4.487895e-8	3.965792e-3	4.627676e-5	1.584609e 0	
16	-1.866815e-4	7.695347e-1	-4.619862e-6	-2.311413e-3	-8.143281e 0
	4.225161e-8	3.692253e-3	4.500860e-5	1.578051e 0	
17	-2.041582e-4	7.640661e-1	-4.320545e-6	-2.207649e-3	-1.079161e 1
	3.826822e-8	3.293581e-3	4.312873e-5	1.570426e 0	

Read -1.866815e-4 as -1.866815×10^{-4}.

Equation of State

For each model level, the density ρ is calculated from T and S by a third–order polynomial approximation to the *UNESCO* [1981] equation of state of sea water:

$$\begin{aligned}\rho = \rho_k^0 \quad + \quad & [c_{k,1} + (c_{k,4} + c_{k,7}S_k^*)S_k^* \\ & + (c_{k,3} + c_{k,8}S_k^* + c_{k,6}T_k^*)T_k^*]T_k^* \\ + \quad & [c_{k,2} + (c_{k,5} + c_{k,9}S_k^*)S_k^*]S_k^*,\end{aligned}$$

where k indicates the model level (= 1, 2, ..., 17), T_k^0, S_k^0, and ρ_k^0 denote the reference temperature, salinity, and density of level k, and $T_k^* = T - T_k^0$ and $S_k^* = (S - S_k^0 - 35)/1000$ give the T and S departures from their respective reference values, the latter being expressed in model salinity units for higher accuracy. The T, S, and ρ reference values may be found in Table A1, and the polynomial's coefficients are listed in Table A2.

Appendix: Symbols and Definitions

Symbols

a	Earth's radius.
g	gravitational acceleration.
$\Omega, f = 2\Omega\sin\phi$	earth's angular velocity, coriolis parameter.
λ, ϕ, z	longitude, latitude, and depth.
$\Delta\lambda, \Delta\phi, \Delta z$	zonal, meridional, and vertical grid spacing.
H	water depth.
Δt	time step.
u, v, w	zonal, meridonal and vertical components of velocity.
Ψ	stream function (vertically integrated mass transport).
$u_{\rm bot}, v_{\rm bot}$	reduced zonal and meridional bottom velocity components.
$u_{S\rm crit}, v_{S\rm crit}$	critical velocities for suspended load transport.
$u_{B\rm crit}, v_{B\rm crit}$	critical velocities for bed load transport.
$w_{\rm sink}$	sinking velocity of sediment particles.
T, S, C	temperature, salinity, and sediment concentration.
ρ, ρ_0	density and mean density of sea water.
ν	kinematic viscosity of sea water
gs, D^*	grain size and sedimentological grain diameter.
FF	form factor of sediment particles.
$\rho_{\rm sed}$	sediment density.
γ	sediment porosity.
$p, p_{\rm surf}$	pressure, surface pressure.
τ^λ, τ^ϕ	zonal and meridional wind stress.

$\tau_B^\lambda, \tau_B^\phi$ zonal and meridional bottom friction. (set to zero in the experiments presented here).

A_{MH}, A_{MV} horizontal and vertical mixing coefficient for momentum: $A_{MH} = 5 \times 10^8 \mathrm{cm^2 s^{-1}}$, $A_{MV} = 1 \mathrm{cm^2 s^{-1}}$.

A_{TH}, A_{TV} horizontal and vertical mixing coefficient for tracers: $A_{TH} = 5 \times 10^6 \mathrm{cm^2 s^{-1}}$, $A_{TV} = 1 \mathrm{cm^2 s^{-1}}$.

Definitions

μ being used as placeholder for T, S, C, u, or v.

μ_t time derivative.

$\mu_\lambda, \quad \mu_\phi, \quad \mu_z$ zonal, meridional, and vertical derivatives.

μ_n derivative normal to boundary.

$$\mathcal{L}(\mu) = \frac{1}{a\cos\phi}[(u\mu)_\lambda + (v\mu\cos\phi)_\phi] + (w\mu)_z$$ three–dimensional advection operator.

$$\mathcal{L}_H(\mu) = \frac{1}{a\cos\phi}[(u\mu)_\lambda + (v\mu\cos\phi)_\phi]$$ two–dimensional advection operator.

$$\nabla^2\mu = \frac{1}{\cos^2\phi}\mu_{\lambda\lambda} + \frac{1}{\cos\phi}(\mu_\phi\cos\phi)_\phi$$ two–dimensional Laplacian operator.

$$\mathcal{D}^u = (A_{MV}u_z)_z + \frac{A_{MH}}{a^2}[\nabla^2 u + (1-\tan^2\phi)u - \frac{2\sin\phi}{\cos^2\phi}v_\lambda]$$

u turbulent mixing operator.

$$\mathcal{D}^v = (A_{MV}v_z)_z + \frac{A_{MH}}{a^2}[\nabla^2 v + (1-\tan^2\phi)v + \frac{2\sin\phi}{\cos^2\phi}u_\lambda]$$

v turbulent mixing operator.

$$\mathcal{D} = (A_{TV}\mu_z)_z + \frac{A_{TH}}{a^2}\nabla^2\mu$$ three–dim. tracer diffusion operator.

$$\mathcal{D}_H = \frac{A_{TH}}{a^2}\nabla^2\mu$$ two–dim. tracer diffusion operator.

$$\mathcal{P}_\lambda = \frac{1}{a\rho_0\cos\phi}p_\lambda, \quad \mathcal{P}_\phi = \frac{1}{a\rho_0}p_\phi$$ zonal and meridional pressure forces.

$\mathcal{C}^\mu$ T and S convective adjustment.

$\mathcal{R}^\mu$ T and S restoring.

$\mathcal{S}$ sediment sources.

Acknowledgments. This work was supported by Deutsche Forschungsgemeinschaft, Special Research Project 313. We thank M. Sarnthein, M. Weinelt, and D. Seidov for data, discussions, and comments, and E. Maier–Reimer for helpful comments in his review.

References

Bitzer, K., and R. Pflug, DEPOD: A three–dimensional model for simulating clastic sedimentation and isostatic compensation in sedimentary basins, in *Quantitative Dynamics Stratigraphy*, edited by T. A. Cross, pp. 335–348, Prentice Hall, Englewood Cliffs, N. J., 1990.

Bryan, K., A numerical method for the study of the circulation of the world ocean, *J. Comput. Phys., 4*, 347–376 1969.

CLIMAP Project Members, The surface of the ice–age Earth, *Science, 191*, 1131–1137, 1976.

Cox, M. D., A primitive equation, 3–dimensional model of the ocean, *GFDL Ocean Group Tech. Rep. 1*, 104 pp., Geophys. Fluid Dyn. Lab./Natl. Oceanic and Atmos. Admin., Princeton Univ., Princeton, N. J., 1984.

Dietrich, G., Atlas of the hydrography of the northern North Atlantic, Conseil international pour l'exploration de la mer, service hydrographique, report, Charlottenlund Slot, Danemark, 1969.

Duplessy, J.–C., L. Labeyrie, A. Juillet–Leclerc, F. Maitre, J. Dupart, and M. Sarnthein, Surface salinity reconstruction of the North Atlantic dur-

ing the Last Glacial Maximum, *Oceanol. Acta, 14*, 311–324, 1991.

Gibbs, R. J., Settling velocity, diameter, and density for flocs of illite, kaolinite, and montmorillonite, *J. Sediment. Petrol., 55*, 65–68, 1985.

Hellerman, S., and M. Rosenstein, Normal monthly wind stress over the world ocean with error estimates, *J. Phys. Oceanogr., 13*, 1093–1104, 1983.

Honjo, S., Particle fluxes and modern sedimentation in the polar oceans, in *Polar Oceanography, Part B*, edited by W. O. Smith Jr., pp. 687–739, Academic, San Diego, Calif., 1990.

Keir, R., K. Stattegger, B. J. Haupt, Chr. Schäfer-Neth, and D. Seidov, Numerische Modelle von Paläoklima, Paläoozeanographie und Sedimentation, in *Berichtsband 91-92-93, Sonderforsch. 313*, pp. 250–280, Univ. Kiel, Kiel, Germany, 1993.

Krohn, J., Ein mathematisches Modell des großräumigen gezeitenbedingten Sedimenttransports mit Anwendung auf die Nordsee, Master thesis, Inst. für Meereskunde, Hamburg, Germany, 1975.

Legutke, S., Modell-Untersuchungen zur Variabilität im Strömungssystem des Europäischen Nordmeeres, *Berichte aus dem Zentrum für Meeres- und Klimaforschung der Universität Hamburg, 4*, 212 pp., 1989.

Levitus, S., *Climatological Atlas of the World Ocean*, 173 pp., NOAA Prof. Pap., *13*, U.S. Government Printing Office, Washington, D. C., 1982.

McCave, I. N., Erosion, transport and deposition of fine-grained marine sediments, in *Fine-Grained Sediments: Deep-Water Processes and Facies*, edited by D. A. Stow and D. J. Piper, pp. 35–69, published for the Geological Society by Blackwell Scientific, Boston, Mass., 1984.

McCave, I. N., and T. F. Gross, In-situ measurements of particle settling velocity in deep sea, *Mar. Geol., 99*, 403–411, 1991.

McCave, I. N., and B. E. Tucholke, Deep current controlled sedimentation in the western North Atlantic, in *The Geology of North America*, vol. M, edited by P. R. Vogt and B. E. Tucholke, pp. 451–468, Geological Society of America, Boulder, Colo., 1986.

Miller, M. C., I. N. McCave, and P. D. Komar, Threshold of sediment motion under unidirectional currents, *Sedimentology, 24*, 507–528, 1977.

Pacanowski, R., K. Dixon, and A. Rosati, The G.F.D.L. Modular Ocean Model Users Guide, Geophys. Fluid Dyn. Lab. Tech. Rep. *2*, Ocean Group, Princeton Univ., Princeton, N. J., 1991,1993.

Pflaumann, Transfer functions "134/6" — A new approach to estimate sea surface temperatures and -salinities of the Eastern North Atlantic from the planctonic foraminifers in the sediment, *Meteor Forschungsergebnisse, Reihe C, 39*, 37–71, 1985.

Puls, W., Numerical simulation of bedform mechanics, *Mitt. Inst. Meereskunde Univ. Hamburg, 24*, 1–147, 1981.

Sarnthein, M., E. Jansen, M. Arnold, J.-C. Duplessy, H. Erlenkeuser, A. Flatoy, T. Veum, E. Vogelsang, and M. S. Weinelt, A time-slice reconstruction of meltwater anomalies at termination I in the North Atlantic between 50 and 80 N, in *The Last Deglaciation: Absolute and Radiocarbon Chronologies, NATO ASI Ser., vol. 12*, edited by E. Bard and W. S. Broecker, pp. 183–200, Springer-Verlag, New York, 1992.

Sarnthein, M., K. Winn, S. Jung, J.-C. Duplessy, L. Labeyrie, H. Erlenkeuser, and G. Ganssen, Changes in East Atlantic deepwater circulation over the last 30000 years: Eight time-slice reconstructions, *Paleoceoanography, 9*, 209–268, 1994.

Stevens, D. P., A numerical ocean circulation model of the Norwegian and Greenland Sea, *Progr. Oceanogr., 27*, 365–402, 1991.

Sündermann J., *North Sea Dynamics*, edited by J. Sündermann and W. Lenz, 693 pp., Springer-Verlag, New York, 1983.

Sündermann, J., and R. Klöcker, Sediment transport modeling with applications to the North Sea, in *North Sea Dynamics*, pp. 453–471, Springer-Verlag, New York, 1983.

UNESCO, *Tenth Report of the Joint Panel on Oceanographic Tables and Standards, vol. 36, Tech. Pap. Mar. Sci.*, 24 pp., New York, 1981.

Wold, C. N., Paleobathymetry and sediment accumulation in the northern North Atlantic and southern Greenland-Iceland-Norwegian Sea, Dissertation, 255 pp., Univ. of Kiel, Kiel, Germany, 1992.

Wold, C. N., Cenozoic sediment accumulation on drifts in the northern North Atlantic ocean, *Paleoceanography*, this issue.

Zanke, U., Berechnung von Sinkgeschwindigkeiten von Sedimenten, *Mitt. Franzius Inst. Wasserbau Küsteningenieurswesen Tech. Univ. Hannover, 46*, 230–245, 1977.

Zanke, U., Zusammenhänge zwischen Strömung und Sedimenttransport, Teil 1, Berechnung des Sedimenttransportes — allgemeiner Fall —, *Mitt. Franzius Inst. Wasserbau Küsteningenieurswesen Tech. Univ. Hannover, 47*, 214–345, 1978.

Bernd J. Haupt, Christian Schäfer-Neth, and Karl Stattegger, Geological-Paleontological Institute and Special Research Project 313, University of Kiel, D-24098 Kiel, Germany. (e-mail: bernd@sfb313.uni-kiel.d400.de; risto@sfb313.uni-kiel.d400.de; karl@sfb313.uni-kiel.d400.de)

(Received April 20, 1994; revised May 12, 1994; accepted June 6, 1994.)